Progress In Electromagnetics Research C, Vol. 62, 99–107, 2016

CPW Dual-Band Antenna Based on Asymmetric Generalized Metamaterial π NRI Transmission Line for Ultra Compact Applications

Mahmoud A. Abdalla* **and Mohamed A. Fouad**

Abstract—In this paper, an ultra compact dual-band metamaterial antenna based on a new asymmetric generalized negative refractive index transmission line is introduced. The antenna was designed to support the 900 MHz GSM and 2400 RFID/WiFi bands. Moreover, the antenna size is only ($15 \times 20\,\text{mm}^2$) which is less than ($0.08\lambda_g \times 0.1\lambda_g$) at the center frequency of the first resonance and ($0.22\lambda_g \times 0.29\lambda_g$) at the center frequency of the second resonance. The theoretical design steps of the antenna are explained. The dual-band antenna design has been validated using equivalent circuit modelling, electromagnetic full wave simulations and practical measurement. The results illustrate that the antenna has the first resonance centred at 0.9 GHz and the second at 2.4 GHz with 15 dB return loss in the two bands. Good agreements among the circuit modelling, electromagnetic full wave simulation and practical measurements have been achieved.

1. INTRODUCTION

Multiband RF components have become very important in modern RF systems. As a consequence, multi-band antennas have been demanded for many wireless services. Metamaterial is an artificial constructed periodic structure characterized with unusual electromagnetic wave propagation properties [1–3]. Metamaterials have been implemented in the microwave band in many configurations. Planar configuration for metamaterials has been suggested by loading planar transmission line (TL) with series capacitors and shunt inductors. This structure is called a negative refractive index (NRI) TL [4] or a composite right/left-handed (CRLH) TL [5]. This TL has a left-handed (LH) passband with anti-parallel phase and group velocities and conventional right-handed (RH) passband. Using this realization, many novel compact and multiband microwave antennas with interesting properties have been proposed [6–10]. Specific examples for compact dual-band antennas are given in [11–15]. Other examples by the authors' group including some attempts to introduce compact dual-band CRLH antennas are presented in different configurations [16–24].

The need for more unique properties leads to the development of extension of the CRLH TL, and the generalized NRI TL (G NRI TL) is presented [25] or extended CRLH TL [26]. This modified metamaterial TL configuration is characterized by multi left-handed bands and multi right-handed bands. Also, related structures are introduced for better performance such as π version [27], all pass one [28] and π-T one [29]. Many researchers have employed these structures making use of these new left-handed properties to design multi-band and compact size components such as coupler [29], power divider [30], phase shifter [31], and filters [32–34]. However, up to our knowledge, only leaky wave antenna based on generalized NRL was suggested [35].

Received 6 December 2015, Accepted 16 February 2016, Scheduled 24 February 2016
* Corresponding author: Mahmoud Abdelrahman Abdalla (maaabdalla@ieee.org).
The authors are with Electromagnetic Fields Group, Electronic Engineering Department, MTC College, Cairo, Egypt.

In this paper, we introduce ultra-compact dual-band antenna based on modified generalized metamaterial NRI TL in CPW configuration for simple realization advantage. The new configuration can be considered as an asymmetric G NRI TL. The antenna designs are based on using only one unit cell of a new modified generalized NRI TL. Hence, a compact size is still a basic feature of the proposed antenna. The proposed antenna has two resonance frequencies. The first one is 0.9 GHz with 5% fraction bandwidth. The second one is 2.4 GHz with 8% fraction bandwidth. These frequency bands were selected as examples for low frequency wireless application, which are interesting in ultra-compact size components. Throughout our work in this paper, we explain the theoretical design principles, circuit modelling, electromagnetic full wave simulations, and finally, the practical experimental measurements have been carried out.

2. ASYMMETRIC G NRL TL AND ANTENNA DESIGN

In this section we introduce the proposed divided asymmetric G NRI TL unit cell, our proposed modified unit cell and the proposed compact antenna based on this configuration. The conventional G NRI TL unit cell and the proposed splitted/asymmetric cell are shown in Fig. 1(a) and Fig. 1(b), respectively. Comparing the two figures, we can notice that the proposed circuit model is converted into asymmetric π configuration. The shunt branch in Fig. 1(a) is divided into two separated branches as shown in Fig. 1(b). It is worth to mention that the two new shunt branches are duplicated so that it introduces symmetric CPW loading in the realization step as will be explained later. Realizing the proposed asymmetric π circuit in CPW configuration needs no via, and hence, it is simpler than microstrip configuration. Moreover, since the proposed asymmetric π G NRI TL configuration has the same order as conventional π G NRI TL, it can support the same number of passbands as the original G NRI TL.

The design of the proposed antenna was achieved in two steps for initial design and further final design. Through the first initial step, the microwave periodic network analysis technique was employed to adjust the two resonance frequencies of the two bands. The specific resonance frequencies are finally re-calculated using the exact transmission line method for optimum return loss. The output in each design step is the lumped values in the circuit model in Fig. 1(b). Next, these values were realized with proper selected distributed elements.

2.1. The Resonance Frequencies Design

Assuming the antenna as a loaded asymmetric G NRI TL, the dispersion equation for antenna equivalent circuit shown in Fig. 1 using the impedance (Z_S, Z_{adds}) and admittances (Y and Y_{sh}) can be obtained using the periodic analysis [36] as

$$\begin{aligned}\cos(\beta d) \;=\; & ((2 + Y_{sh} + 2Y_{sh}Z_{adds} + Z_S Y + Y_{sh}Z_S Y + 2Y_{sh}Z_S Y Z_{adds} \\ & + 2Z_S Y_{sh} + YY_L + 2Y_{sh}YL + Y_{sh}YY_L + 2Y_{sh}YY_L Z_{adds} + Z_{adds}Y)/2) \end{aligned} \quad (1)$$

where β is the propagation phase constant along the proposed dual-band antenna and Y_L the load air admittance $(1/377)\ \Omega^{-1}$.

The initial design for the loading/parasitic inductor and capacitor values is specified by adjusting the resonance frequencies of the proposed dual-band antenna to the limits of the dispersion equation of the π G-NRI TL in (1). There are two resonance frequencies corresponding to $\beta d =$ zero and $\beta d = \pi$. This implies that the left-hand side in Eq. (1) is ± 1. In our design, only one unit cell in Fig. 1(b) is employed. Thus, we have 8 degrees of freedom for different lumped components whereas the solution of Eq. (1) for values ± 1 is only possible for 2 variables.

Accordingly, we have the ability to use 6 values for the parameters. This can help us in selecting the elements so that their realization can be small, and hence an ultra-small size antenna is achieved without affecting the relatively low frequencies. Although the selection in this stage is arbitrary, we have selected these elements based on simple realization aspects. Hence, these variables have been chosen as ($L_S = 4.5$ nH, $C_{HH} = 2.6$ pF, $C_{SH} = 0.2$ pF, $L_{SH} = 5$ nH, $L_{HS} = 0.045$ nH and $C_{HS} = 0.45$ pF). Thus, by solving Eq. (1) for left-hand side $= \pm 1$, the solution values are obtained for ($C_S = 3$ pF and $L_{SH} = 4$ nH).

To confirm the designed values, a dispersion diagram for the employed cell is plotted in Fig. 2. As shown in the figure, the cell has dual-band operation. The first band is a left-handed one that extends

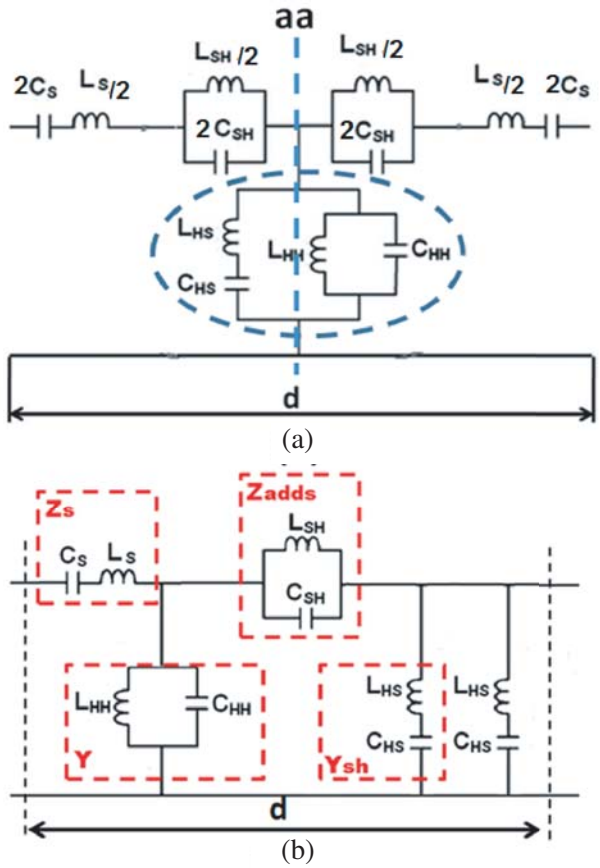

Figure 1. (a) The circuit model of conventional G NRI TL. (b) The circuit model of the proposed new asymmetric π G NRI TL.

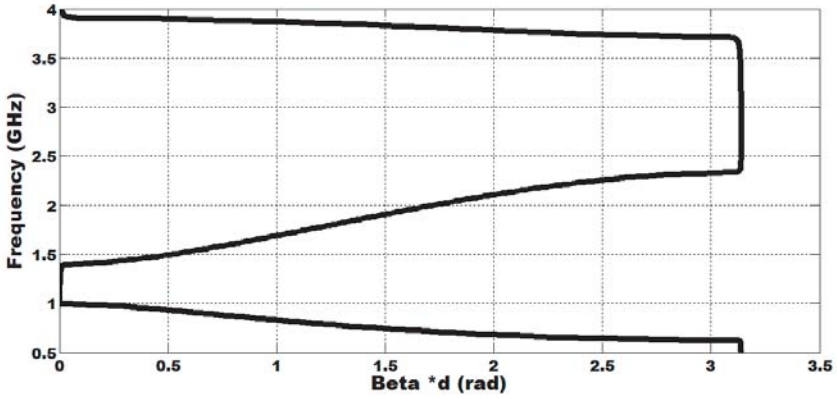

Figure 2. The dispersion diagram for the circuit model of the dual-band antenna.

from 0.55 GHz to almost 1 GHz at which the phase is zero. The second band is a right-handed passband that extends from 1.45 GHz to 2.4 GHz at which the phase is π. Therefore, the resonance condition of the cell to act as a resonant half wavelength antenna can be satisfied at frequencies close to 1 GHz and 2.4 GHz. In the next step of design, this will be tuned to introduce the two resonances at 0.9 GHz and 2.4 GHz.

2.2. The Final Tuning of Antenna Resonances

The second step in the design was the final tuning of antenna resonances based on adjusting the reflection coefficient of the feeding transmission line to be as follow

$$|(S_{11})|_{f_{01},f_{02}} = \left| \frac{2}{A + B/Z_0 + C \times Z_0 + D} \right| = -15\,\text{dB} \tag{2}$$

Equation (2) was solved at the designed resonance frequencies ($f_{01} = 0.9\,\text{GHz}$ and $f_{02} = 2.4\,\text{GHz}$) for the same two elements in the first step. In other words, six parameters were selected based on the same purpose in the initial design step. These elements are the same selected elements in the first with the same values. Next, Eq. (2) was solved numerically using the precalculated values from the initial design step with the initial solution values. Finally, the obtained designed values has been optimized using circuit modelling based on two considerations; first, to achieve the wanted antenna specification illustrated in the beginning of this section and second, the ability to realize. The final lumped values ($C_S = 1.17\,\text{pF}$ and $L_{SH} = 6.55\,\text{nH}$) are examined using circuit modelling, and full wave simulation and experimental measurements will be explained in next sections. It is worth to comment that since the previous explained microwave network analysis requires infinite number of cells, the dispersion phase values were different when we used only one cell. However, this was accepted as an initial solution, and the optimization phases were carried out during full wave simulation in the next section.

3. ANTENNA RESULTS AND DISCUSSION

3.1. Practical Realization

The dual-band antenna is realized in CPW configuration on an FR4 substrate with dielectric constant $\varepsilon_r = 4.4$ and thickness $h = 1.6\,\text{mm}$. The designed lumped elements are based on the antenna circuit mode in Fig. 1(b). The realized CPW dual-band antenna layout is shown in Fig. 3(a), and its fabricated prototype is shown in Fig. 3(b) where compactness is obvious since the antenna length and width are only 1.5 cm and 2 cm. The loading elements are realized using inter digital capacitors, meandered line inductors and strip inductors as follows. The series capacitive load (C_S) is realized by 6 fingers interdigital capacitor with length 4 mm. Two shunt meandered lines with width = 1.3 mm are used to represent the parallel inductance (L_{HH}). One shunt meandered line with width = 2.3 mm is used to represent the inductance (L_{SH}) parallel with the air gap capacitance (C_{sh}) in the series branch. On the other hand, shunt 10 fingers interdigital capacitor with 2.7 mm length representing (C_{HS}) is connected in series with shunt inductance (L_{HS}) which was realized as a metal strip of length 0.4 mm before the interdigital capacitor and 0.6 mm after it. All gaps in the structure equal 0.2 mm, and all transmission lines widths are 0.2 mm. Finally, the antenna radiator is fed by a 50 Ω CPW feeding transmission line

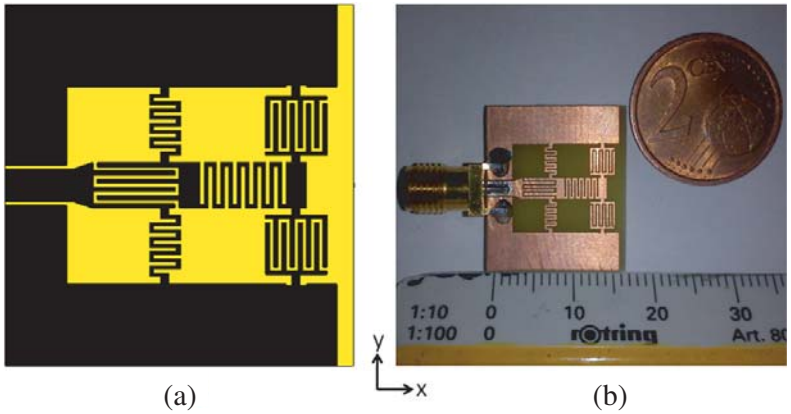

Figure 3. (a) The circuit layout of the proposed dual-band CPW generalized NRI antenna. (b) The fabricated dual-band CPW generalized NRI antenna.

of length 3 mm. The loading elements dimensions were calculated based on the circuit lumped values by using the design formulas in [37, 38].

3.2. Antenna Results

The design verification of the dual-band CPW generalized NRI antenna was checked in two steps. First, the filter design was examined using circuit modeling of the antenna equivalent circuit loaded with 377 Ω load (employing the commercial software advanced system design software). Next, the circuit design results were validated by the full-wave simulation results of the CPW antenna structure employing the commercial finite element software (HFSS) and confirmed by experimental measurement.

The antenna reflection coefficient is measured using vector network analyzer. The different simulated and measured reflection coefficients are shown in Fig. 4. As shown in the figure, there is a good agreement among the three results within the designed resonant bands. Specifically, the full-wave simulation and measurement results agree to very high level. However, there is a difference in the results within the band between 1.2 GHz and 2.2 GHz in the circuit model results in one side and the full wave/measurement simulations on the other side. This can be clarified by observing the difference in the reflection coefficient in this frequency band. In other words, the reflection coefficient is almost constant = −1 dB for the circuit simulation results whereas it highly decreases to below −6 dB for the simulated results. This can be explained as that in circuit model, the equivalent circuit was simulated as a two-port network with matched load at input (port (1)) with 50 Ω and terminated at port (2) with an air impedance (377 Ω). Actually, this assumption is valid only at resonance frequencies; otherwise, this can be accepted. In other words, the circuit model for the one-port antenna as a two-port resonating cell is close to real only at matching. However, this observation is within the stop-band separating the two bands and then it does not violate the message of the antenna performance. The resonant frequencies at both simulations have return loss equal to −16 dB at the first band and −17 dB at the second band center frequencies with good agreement among the three reported results.

The 3D radiation gain patterns at the two operating centre frequencies are plotted in Fig. 5. The antenna demonstrates typical close identical radiation patterns at the two frequencies. The gain of the antenna is quite small at the two operating frequencies (−17 dB at 0.9 GHz and −8 dB at 2.4 GHz). These results can be claimed due to the ultra size reduction of the antenna since the ratio $(ka) = 0.37$ and 1 at 0.9 GHz and 1 at 2.4 GHz, respectively where a is the maximum antenna demission = 20 mm, and k is the free-space wave number.

The maximum of the radiation pattern is positioned along the longitudinal axis of the antenna with minimum at the back lobe pattern. In other words, we can claim that the radiation pattern has an effect of end-fire nature rather than a complete broadside pattern or omnidirectional one. The explanation of the radiation pattern can be understood by investigating the current distribution over the radiating designed metamaterial cell. This is illustrated at the two centre frequencies in Fig. 6. In both cases, the

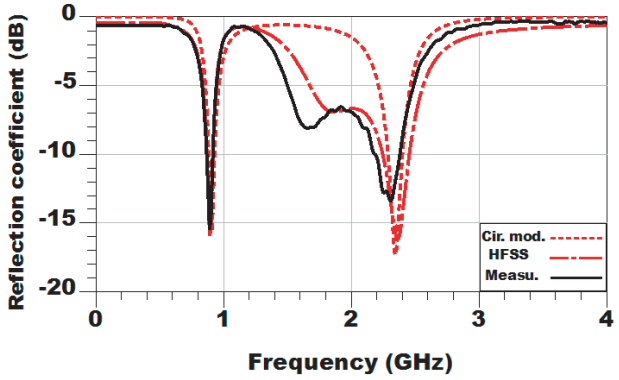

Figure 4. The simulated magnitudes for circuit model, HFSS result and measured reflection coefficient of the proposed dual-band antenna.

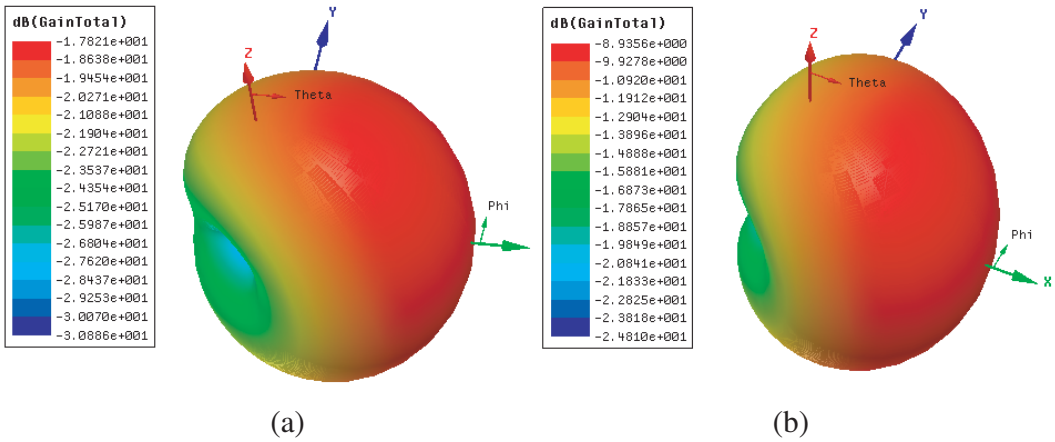

(a) (b)

Figure 5. Proposed antenna 3-D gain, (a) at $f = 900\,\text{MHz}$, (b) at $f = 2.4\,\text{GHz}$.

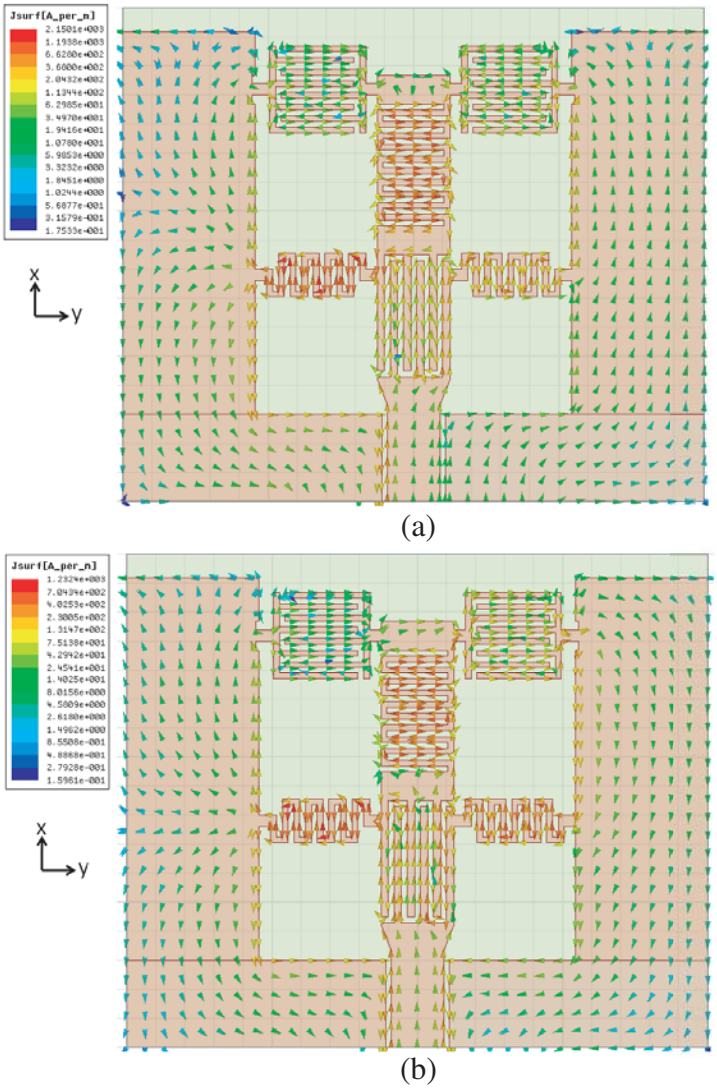

(a)

(b)

Figure 6. The simulated current distribution for the proposed asymmetric G NRI antenna, (a) at 0.9 GHz, (b) at 2.4 GHz.

current is concentrated along the series branch of the asymmetric G NRI TL unit cell. Also, the current is concentrated along the shunt branch of admittance Y in the equivalent circuit model in Fig. 1(b). However, based on the ultra-compact size and small gain of the antenna, the antenna can be applied where the gain is not that essential compared to small size such as implanted applications.

Also, it is worth to comment that by investigating the current distribution in Fig. 6(a), we can notice a reverse in the current direction in the two shunted interdigital capacitors whereas the current in these two capacitors is in the same direction in Fig. 6(b). This can explain the lower gain value at 0.9 GHz than its value at 2.4 GHz.

A comparison between the proposed antenna and recent dual-band compact-size antenna is summarized in Table 1. The comparison demonstrates the ultra-size advantage of the proposed antenna at the expense of a small antenna gain.

Table 1. A comparison between introduced antenna in this paper and recent previous work.

Reference	Frequency Bands	Substrate parameters	Physical Size (mm^2)	Electrical Antenna size (in terms of free space wavelength)
This Work	0.9 GHz	FR4, $\varepsilon_r = 4.4$, Thickness = 1.6 mm	$20 \times 15\,mm^2$	$0.06\lambda_o \times 0.045\lambda_o$
	2.4 GHz			$0.16\lambda_o \times 0.12\lambda_o$
[11]	1.72 GHz	FR4, $\varepsilon_r = 4.4$, Thickness = 1.6 mm	$60 \times 50\,mm^2$	$0.346\lambda_o \times 0.287\lambda_o$
	3 GHz			$0.6\lambda_o \times 0.5\lambda_o$
[12]	2.39 GHz	Taconic, $\varepsilon_r = 3.5$, Thickness = 1.6 mm	$36 \times 35\,mm^2$	$0.53\lambda_o \times 0.52\lambda_o$
	5.33 GHz			$0.64\lambda_o \times 0.62\lambda_o$
[13]	2.62 GHz	FR4, $\varepsilon_r = 4.4$, Thickness = 1.6 mm	$25 \times 20\,mm^2$	$0.218\lambda_o \times 0.175\lambda_o$
	3.23 GHz			$0.27\lambda_o \times 0.215\lambda_o$
[14]	2.62 GHz	FR4, $\varepsilon_r = 4.4$, Thickness = 1.6 mm	$31.7 \times 27\,mm^2$	$0.27\lambda_o \times 0.235\lambda_o$
	3.7 GHz			$0.39\lambda_o \times 0.33\lambda_o$
[15]	0.89 GHz	FR4, $\varepsilon_r = 4.4$, Thickness = 1 mm	$110 \times 60\,mm^2$	$0.326\lambda_o \times 0.178\lambda_o$
	1.94 GHz			$0.71\lambda_o \times 0.387\lambda_o$
[17]	2.4 GHz	Rogers 5880, $\varepsilon_r = 2.2$, Thickness = 1.6 mm	$30 \times 20\,mm^2$	$0.24\lambda_o \times 0.16\lambda_o$
	5.8 GHz			$0.58\lambda_o \times 0.39\lambda_o$
[19]	4.45 GHz	Rogers 5880, $\varepsilon_r = 2.2$, Thickness = 0.508 mm	$33 \times 31\,mm^2$	$0.49\lambda_o \times 0.46\lambda_o$
	7.25 GHz			$0.8\lambda_o \times 0.75\lambda_o$
[20]	3.5 GHz	FR4, $\varepsilon_r = 4.4$, Thickness = 1.6 mm	$26 \times 23\,mm^2$	$0.3\lambda_o \times 0.27\lambda_o$
	5.2 GHz			$0.45\lambda_o \times 0.4\lambda_o$
[21]	2.1 GHz	FR4, $\varepsilon_r = 4.4$, Thickness = 1.6 mm	$20 \times 20\,mm^2$	$0.14\lambda_o \times 0.14\lambda_o$
	2.4 GHz			$0.16\lambda_o \times 0.16\lambda_o$
[23]	1.8 GHz	FR4, $\varepsilon_r = 4.4$, Thickness = 1.6 mm	$95 \times 90\,mm^2$	$0.57\lambda_o \times 0.54\lambda_o$
	2.4 GHz			$0.76\lambda_o \times 0.72\lambda_o$

4. CONCLUSION

A dual-band CPW metamaterial antenna based on asymmetric generalized NRI TL is presented. The antenna analytical design, circuit model, electromagnetic full wave simulations and experimental measurements are introduced. All results have good agreement between each other. The antenna has two resonance frequencies. The first frequency is 0.9 GHz with 5% fraction bandwidth. The second frequency is 2.4 GHz with 8% fraction bandwidth. The antenna size is ultra compact as its length is only $0.08\lambda_g$ at the first band and $0.22\lambda_g$ at the second band. The ultra-small size of the antenna results in low gain, and therefore, it is suitable for indoor and medical applications.

REFERENCES

1. Marqués, R., F. Martín, and M. Sorolla, *Metamaterials with Negative Parameters: Theory, Design and Microwave Applications*, John Wiley & Sons, 2008.
2. Capolino, F., *Theory and Phenomena of Metamaterials*, CRC Press, Oct. 5, 2009.
3. Cui, T. J., D. Smith, and R. Liu, *Metamaterials Theory, Design, and Applications*, Springer, 2010.
4. Eleftheriades, G. V. and K. G. Balmain, *Negative Refractive Metamaterials*, John Wiey & Sons, New Jersey, 2005.
5. Caloz, C. and T. Itoh, *Electromagnetic Metamaterials Transmission Line Theory and Microwave Applications*, John Wiley & Sons, New Jersey, 2006.
6. Caloz, T. I. and A. Rennings, "CRLH metamaterial leaky-wave and resonant antennas," *IEEE Antennas and Propagation Magazine*, Vol. 50, No. 5, 25–39, 2008.
7. Lee, W. H., A. Gummalla, and M. Achour, "Small antennas based on crlh structures: Concept, design, and applications," *IEEE Ant. and Prop. Mag.*, Vol. 53, No. 2, 10–25, 2011.
8. Ziolkowski, R. W., P. Jin, and C. Lin, "Metamaterial-inspired engineering of antennas," *IEEE Proceedings*, Vol. 99, No. 10, 1720–1731, 2011.
9. Dong, Y. and T. Itoh, "Metamaterial-based antennas," *IEEE Proceedings*, Vol. 100, No. 7, 2271–2285, 2012.
10. Mehdipour, A. and G. V. Eleftheriades, "Leaky-wave antennas using negative-refractive-index transmission-line metamaterial supercells," *IEEE Transaction on Antennas and Propagation*, Vol. 62, No. 8, 3929–3942, 2014.
11. Sharma, S. K., D. Gupta, J. D. Mulchandani, and R. K. Chaudhary, "A dumbbell-shaped dual-band metamaterial antenna using FDTD technique," *Progress In Electromagnetics Research Letters*, Vol. 56, 25–30, 2015.
12. Bala, B. D., M. K. A. Rahim, N. A. Murad, and S. K. A. Rahim, "Dual band metamaterial antenna with loaded resonators," *2013 IEEE 2013 Asia-Pacific Microwave Conference Proceedings (APMC)*, 1151–1153, 2013.
13. Sharma, S. K. and R. K. Chaudhary, "Metamaterial inspired dual-band antenna with modified CSRR and EBG loading," *2015 IEEE International Symposium on Antennas and Propagation*, 472–473, Canada, 2015.
14. Si, L. M., W. Zhu, and H. J. Sun, "A compact, planar, and CPW-fed metamaterial-inspired dual-band antenna," *IEEE Antennas and Wireless Propagation Letters*, Vol. 12, 305–308, 2013.
15. Li, L., J. Zhen, F. Huo, and W. Han, "A novel compact multiband antenna employing dual-band CRLH-TL for smart mobile phone application," *IEEE Antennas and Wireless Propagation Letters*, Vol. 12, 1688–1691, 2013.
16. Abdalla, M. A. and Z. Hu, "Compact and tunable metamaterial antenna for multi-band wireless communication applications," *2011 IEEE AP-S Int. Antenna and Propagation Symposium Digest*, 2951–2953, USA, 2011.
17. Abdalla, M. A. and Z. Hu, "Compact dual band meta-material antenna for wireless applications," *2012 Loughborough Antennas & Propagation Conference*, 1–4, UK, 2012.
18. Abdalla, M. A., U. Abdelnaby, and A. A. Mitkees, "Compact and triple band meta-material antenna for all WiMAX applications," *2012 International Symposium on Antennas and Propagation (ISAP)*, 1176–1179, 2012.
19. Ibrahim, W., M. Abdalla, A. Allam, A. Mohamed, and H. Elregeily, "A compact and dual band metamaterial substrate integrated waveguide antenna," *2013 IEEE AP-S International Antenna and Propagation Symposium Digest*, 966–967, USA, 2013.
20. Abdalla, M., "A dual mode CRLH TL metamaterial antenna," *2014 IEEE AP-S International Antenna and Propagation Symposium Digest*, 793–794, Memphis, USA, Jul. 6–11, 2014.
21. Abdalla, M., S. Karimian, and Z. Hu, "Dual band spurious-free SIR metamaterial antenna," *2014 IEEE AP-S International Antenna and Propagation Symposium Digest*, 1005–1006, Memphis, USA, Jul. 6–11, 2014.

22. Abdalla, M., M. Fouad, A. Ahmed, and Z. Hu, "A new compact microstrip triple band antenna using half mode CRLH transmission line," *2013 IEEE AP-S Int. Antenna and Propagation Symposium Digest*, 634–635, USA, 2013.
23. Abdalla, M., M. A. El-Dahab, and M. Ghouz, "Dual/triple band printed dipole antenna loaded with CRLH cells," *2014 IEEE AP-S International Antenna and Propagation Symposium Digest*, 1007–1008, USA, 2014.
24. Abdalla, M. and A. Ibrahim, "Multi-band meta-material antenna with asymmetric coplanar strip-fed structure," *2015 IEEE AP-S International Antenna and Propagation Symposium Digest*, 631–632, Canada, 2015.
25. Eleftheriades, G. V., "A generalized negative-refractive-index transmission-line (NRI-TL) metamaterial for dual-band and quad-band applications," *IEEE Microw. Wireless Compon. Lett.*, Vol. 17, No. 6, 415–417, 2007.
26. Rennings, A., S. Otto, J. Mosig, C. Caloz, and I. Wolff, "Extended composite right/left-handed (E-CRLH) metamaterial and its application as quadband quarter-wavelength transmission line," *Asia-Pacific Microwave Conference (APMC)*, 1405–1408, Japan, Dec. 2006.
27. Ryan, C. and G. Eleftheriades, "Design of a printed dual-band coupled-line coupler with generalised negative-refractive index transmission lines," *IET Microwaves, Antennas & Propagation*, Vol. 6, 705–712, 2012.
28. Ryan, G. M. and G. V. Eleftheriades, "A single-ended all-pass generalized negative-refractive-index transmission line using a bridged-T circuit," *Microwave 2012 IEEE MTT-S International Symposium Digest (MTT)*, 1–3, Canada, 2012.
29. Fouad, M. A. and M. A. Abdalla, "A new π-T generalized metamaterial NRI transmission line for a compact CPW triple BPF applications," *IET Microwave, Antenna and Propagation*, Vol. 8, No. 9, 1–8, Jun. 2014.
30. Papanastasiou, A. C., G. E. Georghiou, and G. V. Eleftheriades, "A quad-band Wilkinson power divider using generalized NRI transmission lines," *IEEE Microwave and Wireless Components Letters*, Vol. 18, No. 8, 521–523, 2008.
31. Markley, L. and G. V. Eleftheriades, "Quad-band negative-refractive-index transmission-line unit cell with reduced group delay," *Electronics Letters*, Vol. 46, No. 17, 1206–1208, 2010.
32. Studniberg, M. and G. V. Eleftheriades, "A dual-band bandpass filter based on generalized negative-refractive-index transmission-lines," *IEEE Microwave and Wireless Components Letters*, Vol. 19, No. 1, 18–20, 2009.
33. Fouad, M. and M. Abdalla, "A compact and new CPW dual BPF based on generalized metamaterial CRLH transmission line," *2013 IEEE AP-S Int. Antenna and Propagation Symposium Digest*, 628–629, USA, 2013.
34. Fouad, M. A. and M. A. Abdalla, "Ultra compact CPW dual band filter based on Π-generalized metamaterial NRI transmission line," *Journal of Electromagnetic Waves and Applications*, Vol. 29, No. 8, 1093–1103, 2015.
35. Ryan, C. G. M. and G. V. Eleftheriades, "A dual-band leaky-wave antenna based on generalized negative-refractive-index transmission-lines," *2010 IEEE Antennas and Propagation Society International Symposium*, 1–4, 2010.
36. Pozar, D. M., *Microwave Engineering*, J. Wiley & Sons, New York, 1998.
37. Bahl, I. J., *Lumped Elements for RF and Microwave Circuits*, Artech House, Boston London, 2003.
38. Hong, J. and M. J. Lancaster, *Microstrip Filters for RF Microwave Applications*, John Wiley & Sons, New York, 2001.